



**HAL**  
open science

## Sensitive and transportable gadolinium-core plastic scintillator sphere for neutron detection and counting

Jonathan Dumazert, Romain Coulon, Frédérick Carrel, Gwenolé Corre, Stéphane Normand, Matthieu Hamel, Laurence Méchin

### ► To cite this version:

Jonathan Dumazert, Romain Coulon, Frédérick Carrel, Gwenolé Corre, Stéphane Normand, et al.. Sensitive and transportable gadolinium-core plastic scintillator sphere for neutron detection and counting. Nuclear Instruments and Methods in Physics Research Section A: Accelerators, Spectrometers, Detectors and Associated Equipment, 2016, 828, pp.181 - 190. 10.1016/j.nima.2016.05.054 . hal-01615195

**HAL Id: hal-01615195**

**<https://hal.science/hal-01615195>**

Submitted on 29 Apr 2022

**HAL** is a multi-disciplinary open access archive for the deposit and dissemination of scientific research documents, whether they are published or not. The documents may come from teaching and research institutions in France or abroad, or from public or private research centers.

L'archive ouverte pluridisciplinaire **HAL**, est destinée au dépôt et à la diffusion de documents scientifiques de niveau recherche, publiés ou non, émanant des établissements d'enseignement et de recherche français ou étrangers, des laboratoires publics ou privés.

# Sensitive and transportable gadolinium-core plastic scintillator sphere for neutron detection and counting

Jonathan Dumazert<sup>1</sup>, Romain Coulon<sup>1</sup>, Frédéric Carrel<sup>1</sup>, Gwénéolé Corre<sup>1</sup>, Stéphane Normand<sup>1</sup>, Laurence Méchin<sup>2</sup> and Matthieu Hamel<sup>1</sup>.

<sup>1</sup>CEA, LIST, Laboratoire Capteurs Architectures Electroniques, 91191 Gif-sur-Yvette, France.

<sup>2</sup>CNRS, UCBN, Groupe de Recherche en Informatique, Image, Automatique et Instrumentation de Caen, 14050 Caen, France.

**Abstract** – Neutron detection forms a critical branch of nuclear-related issues, currently driven by the search for competitive alternative technologies to neutron counters based on the helium-3 isotope. The deployment of plastic scintillators shows a high potential for efficient detectors, safer and more reliable than liquids, more easily scalable and cost-effective than inorganic. In the meantime, natural gadolinium, through its 155 and mostly 157 isotopes, presents an exceptionally high interaction probability with thermal neutrons. This paper introduces a dual system including a metal gadolinium core inserted at the center of a high-scale plastic scintillator sphere. Incident fast neutrons are thermalized by the scintillator shell then may be captured with a significant probability by gadolinium 155 and 157 nuclei in the core. The deposition of a sufficient fraction of the capture high-energy prompt gamma signature inside the scintillator shell will then allow discrimination from background radiations by energy threshold, and therefore neutron detection. The scaling of the system with the Monte Carlo MCNPX2.7 code was carried out according to a tradeoff between the moderation of incident fast neutrons and the probability of slow neutron capture by a moderate-cost metal gadolinium core. Based on the parameters extracted from simulation, a laboratory prototype for the assessment of the detection method principle has been synthesized. The robustness and sensitivity of the neutron detection principle are then assessed by counting measurement experiments. Experimental results confirm the potential for a stable, highly sensitive, transportable and cost-efficient neutron detector and orientate future investigation toward promising axes.

## I. INTRODUCTION

NEUTRON counting forms a critical branch of nuclear-related issues, whether flow monitoring on industrial infrastructures [1,2], dose rate monitoring for radioprotection [3] or radiological material detection addressing CBRN threats [4] are concerned. More specifically, the last decade has been driven by the quest for competitive alternative technologies to neutron counters based on the helium-3 isotope whose announced worldwide shortage has generated massive market value fluctuations [5]. Among alternative stable elements, gadolinium, through its naturally present 155 and (especially) 157 isotopes, exhibits the largest cross section (48890 barns) for the absorption of incident neutrons within the thermal energy range. However, a technical conundrum lies within the separation of the scintillation signal due to the prompt gamma rays most significantly emitted posterior to the  $(n,\gamma)$  neutron radiative capture from the scintillation signal attributable to ambient gamma-rays. In particular, amplitude discrimination between the high-energy prompt gamma-ray signature of the capture and the radiation background requires for a significant fraction of this signature to be absorbed inside the sensor. Now the synthesis of plastic scintillators shows a high potential for the deployment of efficient, scalable and cost-effective detectors [6]. In default of any available Pulse-Shape Discrimination (PSD), the authors therefore propose a gadolinium-based neutron counting scheme using high-scale plastic scintillators optimized for neutron moderation and the absorption of high-energy gamma-rays from the  $(n,\gamma)$  capture.

## II. RELATED WORK

Neutron detection represents a long-term technological challenge due to the indirectly ionizing nature of the radiation: the secondary particles generated after an interaction between a neutron and an atom of the sensor, which carry a charge, actually form the signature of the neutron passage. It is additionally imperative, when monitoring neutron activity, to discriminate this signature against the signal generated by secondary particles generated through the interaction between background photon radiations and the electrons of the sensor atoms.

Among the detectors specifically dedicated to thermal neutrons, helium-3 counters, which exploit a highly neutron/gamma discriminative  $(n,p)$  type reaction with a thermal cross section equal to 5327 barns, are the most widespread [7]. The physical sensor is typically integrated into a radioprotection neutron dose monitoring system combining the moderation of incident neutrons inside a moderator, such as a Bonner sphere [8] whose thickness and geometry are optimized according to the targeted application, and a helium-3 core in which thermal neutrons are subsequently captured. Given the announced global shortage and strategic issues regarding tritium, alternative technologies to helium-3 are actively investigated, notably among liquid and plastic scintillators [9]. Mares et al. have for instance adapted the principle of a Bonner moderator shell, replacing the helium-3 internal proportional counter by an inorganic lithium-6 iodide scintillator [10]. The authors then make use of the 950-barn cross section of lithium-6 for the  $(n,\alpha)$  capture of thermal neutrons. The main advantage of lithium-6, which is balanced by its lesser cross

45 section, comes from an available discrimination of the resulting alpha signature against any photon background based of the  
46 shape of pulses (PSD).

47 Natural gadolinium (Gd) exists in the form of a combination of isotopes among which gadolinium-155 (14.7 % proportion,  
48 61000 barns cross section) and mostly gadolinium-157 (15.68 %, 255000 barns) present an exceptionally high interaction  
49 probability with thermal neutrons [11]. Gadolinium is implemented in scintillator-based neutron detectors and counters, for  
50 instance in lithium-gadolinium-borate inorganic scintillators [12]. An alternative to such crystals has been presented under the  
51 form of ceramic crystals into which a gadolinium oxide has been inserted [13,14]. The limits associated with inorganic  
52 scintillators, notably in terms of manufacturing costs, scalability and shape-flexibility, justify the search for concurrent options.  
53 Structures presenting fiber networks including a gadolinium glass [15] have been divulged, which allow a scale-up without  
54 exceeding the cost of a helium-3 counter. On the other hand, reusing a Bonner-type spherical shell, Beil et al. [16] have  
55 conceived a neutron detector into which the central helium-3 counter is replaced by a gadolinium-loaded liquid scintillator core.  
56 However liquid scintillators raise safety issues due to a low flash point and the potential leakage of toxic materials.

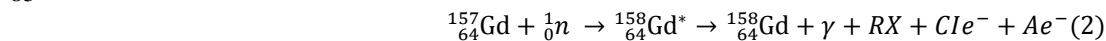
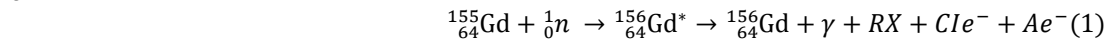
57 The limitations of concurrent technologies have led to the deployment of plastic scintillators [17] which are low-cost (contrary  
58 to inorganic scintillators) easily scalable and shape-flexible, safer than their liquid counterparts due to their higher flash point.  
59 Nanoscintillator-based systems into which gadolinium is notably inserted under the form of garnet, halide or oxide, have been  
60 patented [18]. Additionally, low-scale gadolinium-loaded scintillators compensated by same-volume bismuth-loaded plastic have  
61 shown promising neutron sensitivities in medium and high-energy gamma backgrounds [19]. The most conventional approach in  
62 recent work, after comparison between the dispersion of gadolinium crystal spheres into the plastic matrix and the interleaving of  
63 gadolinium foils between plastic blocks [20] tends to favor the second option. As a result, the principle of wrapping inorganic  
64 scintillators with gadolinium foils, which was patented by Richard [21], has been transposed to systems in which the scintillator  
65 takes the form of plastic scintillator bars [22]. Similarly, systems presented as lithium-6 iodide scintillator lines interleaved  
66 between hydrogenous blocks which moderate incident neutrons, patented by Polichar et al. [23], find an analogue in the  
67 prototype named *Gadolinium-lined plastic scintillator detector* and introduced in the course of the SCINTILLA FP7 European  
68 project [24]. The authors have divulged a detection system using the radiative capture of moderated neutrons in optimized planar  
69 gadolinium foils interleaved between large parallelepiped plastic scintillator blocks, concatenated to form high-volume Radiation  
70 Portal Monitors addressing CBRN threats.

### 71 III. PRINCIPLE OF THE DETECTION AND COUNTING METHOD

72 The principle of the neutron activity monitoring system hereby disclosed is currently under patent deposition [25] and has  
73 been trademarked under the name Gadosphere™. The dual system includes a metal or oxide gadolinium core inserted at the  
74 center of a high-scale plastic scintillator sphere. Incident fast neutrons are thermalized by the hydrogenous nature of the  
75 scintillator shell then may be captured with a significant probability by gadolinium-155 and 157 nuclei inside the core. The  
76 deposition of a sufficient fraction of the capture high-energy prompt gamma signature inside the scintillator shell will then allow  
77 amplitude discrimination from background radiations leading to neutron detection.

#### 78 A. High-energy prompt gamma signature of thermal neutron radiative capture by gadolinium-157 and gadolinium-155

79 The prompt source term associated with the de-excitation of a gadolinium nucleus following the absorption of a thermal  
80 neutron is subdivided into a prompt photon source term and a prompt electron source term. The complete equations of the  
81 nuclear reactions are presented in (1) and (2), where the sum of the gamma-rays labeled  $\gamma$  and the X-rays noted  $RX$  forms the  
82 photon source term, and the sum of internal conversion electrons noted  $Cle^-$  and the labeled Auger electrons  $Ae^-$  forms the  
83 electron source term.  
84



87 The detection scheme aims at exploiting the high-energy prompt gamma-ray signature of the capture. With this regard, an  
88 energy threshold set above 3 MeV would exceed the most energetic gamma-rays found in the thorium-232 chain [26] and  
89 therefore theoretically rid the measurement of background activity, provided that pile-up is limited and no fission product is  
90 present. The relevant signature [27] represents 1.299 gamma-rays emitted between 3.0606 and 7.85767 MeV per  ${}^{157}_{64}\text{Gd}(n, \gamma)$   
91 radiative capture, and 0.2464 gamma-rays between 3.9014 and 6.76483 MeV per  ${}^{155}_{64}\text{Gd}(n, \gamma)$  capture, which, in a conveniently  
92 scaled sensor, may lead to significant energy deposition exceeding 3 MeV. Fig. 1 and Fig. 2 respectively reproduce the prompt  
93 gamma-ray de-excitation spectra of the  ${}^{157}_{64}\text{Gd}(n, \gamma)$  and  ${}^{155}_{64}\text{Gd}(n, \gamma)$  captures above 3 MeV.  
94

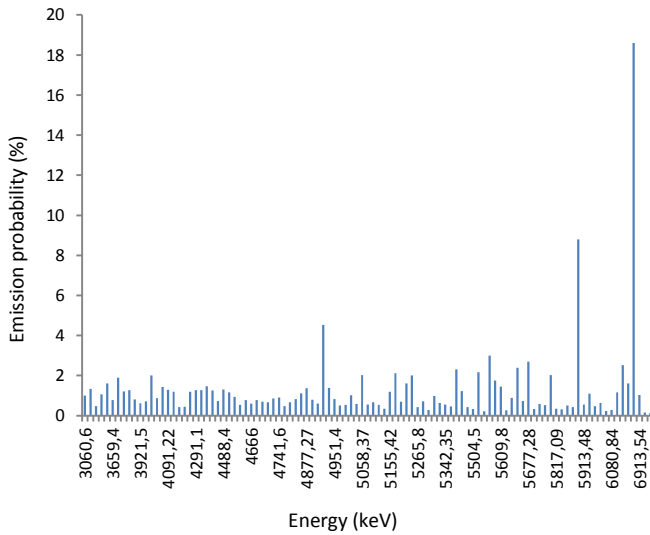


Fig. 1. Prompt gamma-ray de-excitation spectra of the  $^{157}_{64}\text{Gd}(n, \gamma)$  above 3 MeV

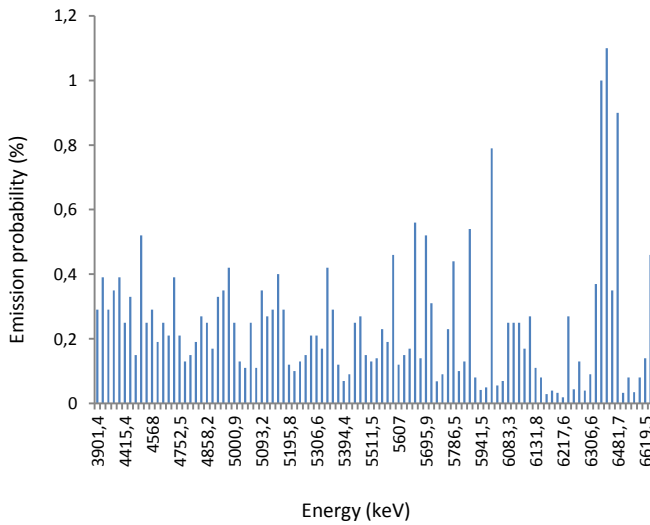


Fig. 2. Prompt gamma-ray de-excitation spectra of the  $^{155}_{64}\text{Gd}(n, \gamma)$  above 3 MeV

### B. Detail of the system and electronics

The physical sensor, illustrated in Fig. 3, is composed of a metal gadolinium core (1) positioned at the center of a spherical plastic scintillator shell (2). A spherical geometry has been chosen as it minimizes anisotropy biases in counting process [25]. The respective scaling of (1) and (2) is critical for the maximization of the collected signal, as the simulation presented in Part IV will demonstrate, so that, for every active volume of the core, one optimal diameter for the surrounding shell may be found.

The core (1) is filled in a suitable receptacle (3) which also plays the part of a reflector for the scintillation photons generated inside (2). In order to minimize the escape of scintillation photons, a white paint reflector (4) covers the surface of the shell, except for the interface with the photon-electron conversion system (5). The conversion system takes the form of a photomultiplier powered by a high voltage supply (6) in order to multiply the charges.

The processing of the signal exiting (5) is performed by a dedicated electronic chain (7) connected to a computer (8). The electronics include a triggering of the pulse, the evaluation of its maximum and, after a comparison to a relevant amplitude threshold set from previous calibration, the deliverance of an all-or-nothing signal. With a temporal step labeled  $\Delta t$ , a counter is incremented from the all-or-nothing signal, then providing an estimate of the counting rate  $\lambda$ .

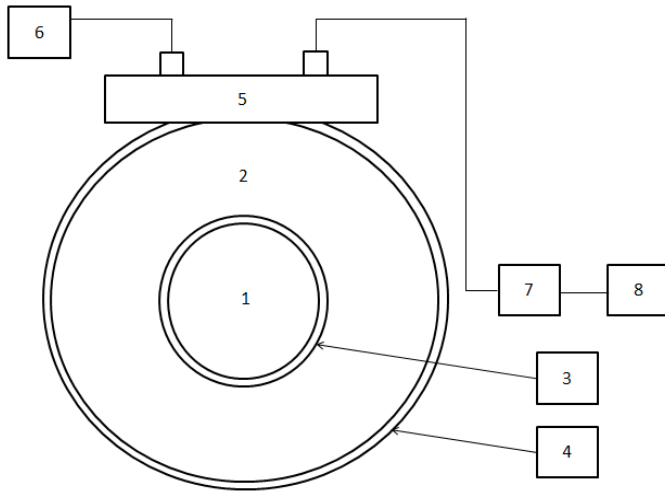


Fig. 3. Principle sketch of the counting system.

#### IV. SIMULATION-BASED SCALING OF THE DUAL SENSOR

The scaling of the dual sensor was carried out by simulations using the probabilistic Monte Carlo MCNPX2.7 code for particle transport [28]. The program provides a complete historical on every generated corpuscle, for source terms as well as for diffusion products, until its energy falls below a 1 keV threshold.

A spherical geometry according to Fig. 3 was retained. The modeled 100 % pure natural gadolinium core takes the simplified form of a  $7.901 \text{ g.cm}^{-3}$  volumic mass sphere of fixed radius  $r = 0.7 \text{ cm}$ , hence an approximate 11 grams mass chosen for the practical realization out of preliminarily assessed compromise between achievable neutron sensitivity and cost-efficiency. The plastic scintillator shell is represented by a  $1.07 \text{ g.cm}^{-3}$  density 91.3 % wt carbon and 7.7 % wt hydrogen sphere using the benz.01t material card to account for the styrene structure of the matrix. The shell radius  $R$  is a variable according to which the maximization of the interaction rate useful for the detection must be carried out. The reflectors described in subsection III.B. are neglected in this first-order model.

A neutron-emitting californium-252 source was simulated using the set of constants describing its Watt spectrum and furnished by the literature [29]. The source is positioned at a distance  $d = 20 \text{ cm}$  of the closest point on the scintillator shell surface.

The flux tally 4 of the MCNPX2.7 code coupled with the multiplier 102 FM card provides a radiative capture rate per gadolinium isotope for the fission neutrons emitted by the source, which we express in capture per neutron ( $\text{ca.n}^{-1}$ ). These capture rates are respectively labeled  $\tau_{ca,157}$  and  $\tau_{ca,155}$  for the 157 and 155 nuclei inside the core. The measurand is limited to scintillation photons induced by energy depositions superior to a 3 MeV threshold inside the plastic shell from prompt gamma-rays of energy exceeding 3 MeV, emitted with a  $\tau_{E>3 \text{ MeV},157} = 1.299$  gamma per capture ( $\gamma.\text{ca}^{-1}$ ) rate in the radiative de-excitations of gadolinium-157 and with a  $\tau_{E>3 \text{ MeV},155} = 0.2464$  gamma per capture ( $\gamma.\text{ca}^{-1}$ ) rate in the radiative de-excitations of gadolinium-155. Both gamma-rays distributions are fully simulated using the prompt source terms from the IAEA database [27]. The homogenous spatial distribution for de-excitation source terms was limited to the 0.1 cm shell of the gadolinium core closest to the plastic, as previous simulations have shown that 97 % of neutron radiative captures occur within this volume. Eventually, using the deposition pulse height tally 8 of the MCNPX2.7 code, the rate of prompt gamma-rays actually depositing at least 3 MeV inside the plastic scintillator in deposition per gamma ( $\text{d.}\gamma^{-1}$ ) is derived. These rates are respectively labeled  $\tau_{D>3 \text{ MeV},157}$  and  $\tau_{D>3 \text{ MeV},155}$  for the de-excitation high-energy source terms associated with gadolinium-157 and 155.

The overall  $\tau$  interaction rate useful for the detection reads as computed from (3) and is expressed in theoretical counts per fast neutron ( $\text{c.n}^{-1}$ ).

$$\tau = \tau_{ca,157} \cdot \tau_{E>3 \text{ MeV},157} \cdot \tau_{D>3 \text{ MeV},157} + \tau_{ca,155} \cdot \tau_{E>3 \text{ MeV},155} \cdot \tau_{D>3 \text{ MeV},155} \quad (3)$$

The simulation study shows that, for a set core size, beyond a given radius for the scintillator sphere, the adjuvant moderation of incident neutrons is balanced by the spatial dispersion of the thermalized neutrons, which then reach the core with lesser probabilities. On the other hand the fraction of energy deposited by de-excitation high-energy gamma rays increases monotonously with the scintillator radius. *In fine*, the scaling of the dual detection system is a result of a tradeoff between these antagonistic trends. The evolution of  $\tau$  as a function of the shell radius  $R$  confirms the existence of an optimal range for the shell radius, lying between  $R = 12 \text{ cm}$  and  $R = 15 \text{ cm}$ . Under this consideration, a commercial 6-liter spherical mold with a 11.8 cm radius was selected for the realization of a laboratory prototype described *infra*.

A. Preparation of the plastic scintillator

The preparation of high-scale plastic scintillators poses various challenges as far as turbidity, self-absorption, stability and homogeneity may be concerned [30]. A laboratory prototype for the assessment of the counting method performance has been synthesized. In a 6-liter spherical mold were added the following components of the plastic scintillator shell: the styrene monomer, a reticulating agent, 2,5-diphenyloxazole (PPO) as a primary fluorophore and 1,4-Bis(5-phenyl-2-oxazolyl)benzene (POPOP) as a secondary fluorophore, whose topological representations are given in Fig. 4. Both fluorophores, added at a standard concentration, dissolve easily in the liquid monomer mixture. After a preliminary process of purification of chemicals, the resulting solution was put under a nitrogen atmosphere, bubbled for approximately one hour. An 11 grams 99.9 % pure metal gadolinium ingot from Strem Chemicals [31] was subsequently added at the center of the mold. The system purged once again with argon, was sealed and placed into an oven at a precise heating cycle for 40 days. Once complete polymerization was observed, the mold was cooled down to room temperature and shattered. The scintillator surface in contact with the photo-detection cell was polished and the rest of the shell was covered with a white reflecting paint in view of the detection experiment.

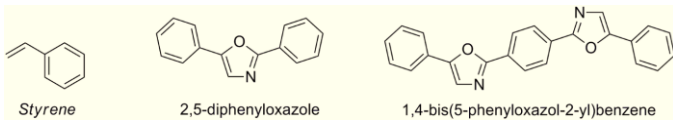


Fig. 4. Topological representations of molecules.

B. Acquisition and measurement setup

The scintillator is coupled to a bialkali photocathode of a Hamamatsu™ H1949-51 model photomultiplier (PMT) powered by a CAEN N147 model 4CH HV programmable power supply. A custom made electronics developed at the CEA List [32] and devoted to the processing of short scintillation pulses (rise and decay time within the nanosecond time scale) digitizes the signal at a frequency equaling  $200\text{Msample}\cdot\text{s}^{-1}$ , performs a filtering of the signal over 7 samples in order to maximize the signal-to-noise ratio (SNR) and a differentiation to correct base line fluctuations, triggers the pulse and determines its maximal amplitude to store the event into a 8-bit pulse height histogram. The photomultiplier is isolated from ambient light and static noise sources inside an opaque Faraday cage. The counting measurement setup, including the PMT and the plastic scintillator sphere, is depicted in Fig. 5, while Fig. 6 presents the acquisition card.

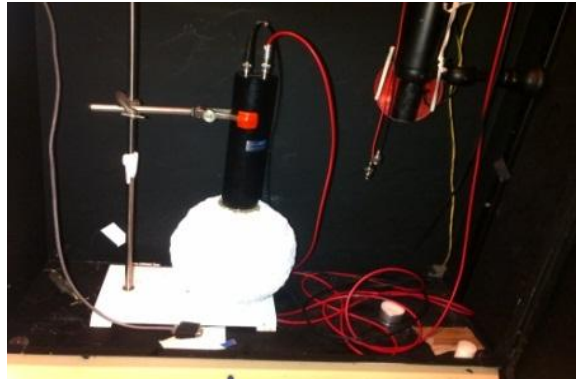


Fig. 5. Experimental measurement setup



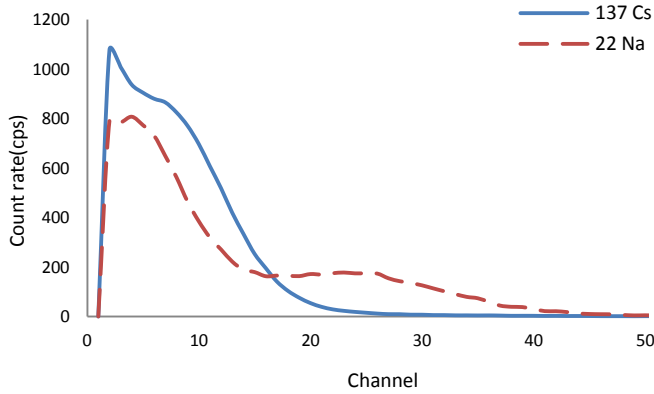
Fig. 6. Acquisition card.

C. Linear calibration of the scintillator response

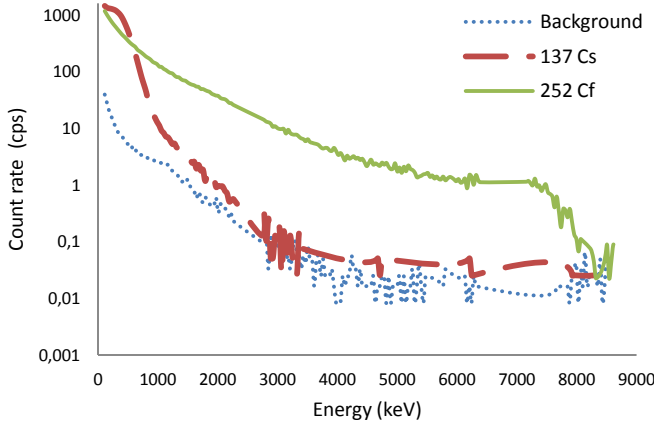
- A high-energy calibration of the scintillator response was performed using:
- a sodium-22 source of activity  $A = 4 \text{ MBq}$  positioned at a distance  $d = 30 \text{ cm}$  of the closest point on the scintillator surface, at a height  $h = 11.8 \text{ cm}$ , whose second Compton edge was observed at  $1061 \text{ keV}$ ;

193 - a cesium-137 source of activity  $A = 34$  MBq positioned at a distance  $d = 100$  cm of the closest point on the scintillator  
194 surface, at a height  $h = 11.8$  cm, whose Compton edge was observed at 478 keV;

195 Using the protocol of Bertolaccini et al. [33], these energies were identified to the channel numbers corresponding to 80 % of  
196 the maximum spectrum values, which may be read on the spectra reproduced in Fig. 7. Knowing that the response of the  
197 scintillator is linear for high energies [34], a conversion coefficient from channel number to energy equal to  $36.5 \text{ keV}\cdot\text{channel}^{-1}$   
198 was computed. Typical spectra posterior to calibration are presented for the background of the experiment room, exposure to a  
199 cesium-137 and a californium-252 source in Fig. 8. As predicted by the model, a significant high-energy component of the  
200 spectrum distinguishes the response of the dual sensor to the neutron-emitting source.  
201



202 Fig. 7. Sodium-22 and cesium-137 spectra for high-energy calibration



205 Fig. 8. Pulse height spectra acquired with custom-made electronics

## 207 VI. EXPERIMENTAL RESULTS

### 208 A. Background measurements

209 The gamma and neutron backgrounds of the measurement room are respectively measured equal to  $0.1 \mu\text{Sv}\cdot\text{h}^{-1}$  and  $0.01$   
210  $\mu\text{Sv}\cdot\text{h}^{-1}$  with a commercial Thermo Electron ESM FH 40G-L 10 radiometer and a commercial LB 6411 Neutron Probe. In this  
211 background and in the absence of any neutron, a significantly non-null count rate is displayed by the laboratory prototype, whose  
212 evolution as a function of the counting threshold is reproduced in Fig. 9.  
213

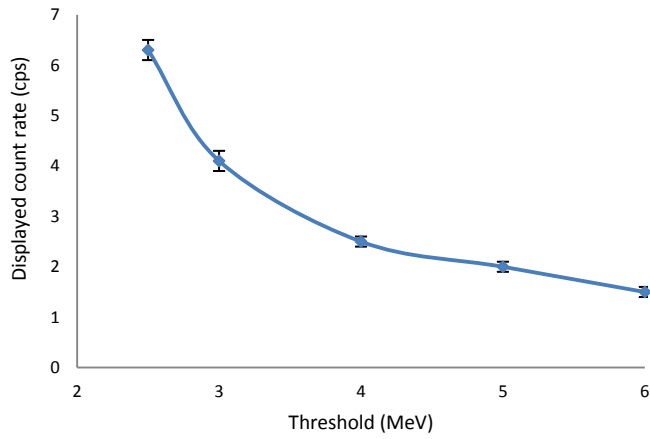


Fig. 9. Background count rate (cps)

214  
215

216 *B. Stability curves*

217 In order to determine, for a given gamma-ray background, the relevant counting threshold, stability curves have to be  
 218 constructed. A californium-252 source of activity  $A = 784 \text{ kBq}$  is positioned at a distance  $d = 60 \text{ cm}$  of the closest  
 219 point on the scintillator surface, at a height  $h = 11.8 \text{ cm}$ . At this distance, the gamma dose rate from the californium-  
 220 252 source at the scintillator surface is measured equal to  $0.1 \mu\text{Sv}\cdot\text{h}^{-1}$ , therefore confounded with the room background.  
 221 Additionally, two gamma-ray backgrounds are introduced using:

- 222 - a cesium-137 source of activity  $A = 34 \text{ MBq}$ , positioned at a height  $h = 11.8 \text{ cm}$  and whose distance is varied to  
 223 generate dose rates ranging from  $0.7$  to  $60 \mu\text{Sv}\cdot\text{h}^{-1}$  at the closest point on the scintillator surface;
- 224 - a cobalt-60 source of activity  $A = 184 \text{ kBq}$ , positioned at a height  $h = 11.8 \text{ cm}$  and whose distance is varied to generate  
 225 dose rates ranging from  $0.6$  to  $35 \mu\text{Sv}\cdot\text{h}^{-1}$  at the closest point on the scintillator surface.

226 The stability curves displayed in Fig. 10 and Fig. 11 present, for the cesium-137 and the cobalt-60 backgrounds respectively,  
 227 the evolution of the count rate as a function of the gamma dose rate and the counting threshold.  
 228

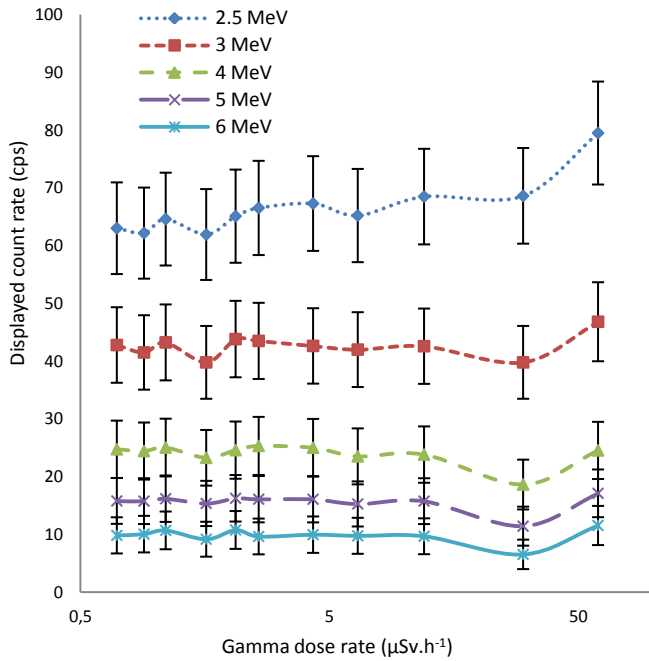


Fig. 10. Stability curves in presence of a cesium-137 background

229  
230  
231

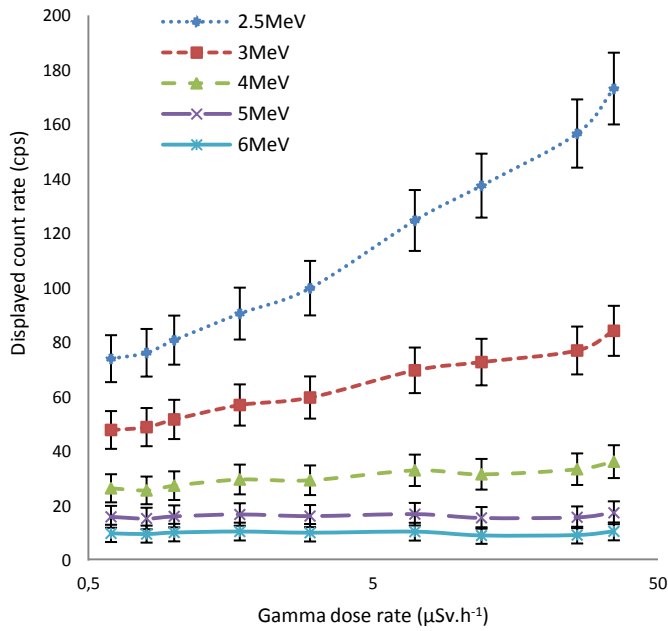


Fig. 11. Stability curves in presence of a cobalt-60 background

The characteristics show that in presence of a cesium-137 type background ranging from 0.7 to 60  $\mu\text{Sv}\cdot\text{h}^{-1}$ , a stable count rate within one standard deviation of the Poisson uncertainty is displayed from a 3 MeV counting threshold. However, in presence of a higher-energy cobalt-60 background ranging from 0.6 to 35  $\mu\text{Sv}\cdot\text{h}^{-1}$ , due to gamma pile-up, such stability is solely ensured from a 5 MeV counting threshold. Both counting thresholds will be retained for the evaluation of sensitivity in their respective backgrounds, ensuring an unbiased counting up to at least several tens of micro-Sieverts per hour.

### C. Neutron sensitivity

The same californium-252 source is positioned at a distance  $d = 60$  cm of the closest point on the scintillator surface, at a height  $h = 11.8$  cm, without any additional gamma-ray emitter. Count rates equaling  $\lambda = 34.1 \pm 5.8$  cps and  $13.0 \pm 3.6$  cps are respectively recorded over 3 MeV (counting threshold to account for a possible cesium-137 type background up to 60  $\mu\text{Sv}\cdot\text{h}^{-1}$ ) and 5 MeV (counting threshold to account for a possible cobalt-60 type background up to 35  $\mu\text{Sv}\cdot\text{h}^{-1}$ ). We label  $A = 784$   $\text{kf}\cdot\text{s}^{-1}$  the number of fissions per second and  $\nu = 3.73$   $\text{n}\cdot\text{f}^{-1}$  the mean number of neutrons emitted per fission [35]. The sensor section is noted  $\Sigma = \pi R^2$ , where  $R = 11.8$  cm is the scintillator radius. The ratio of solid angles from the isotropic emission of the source approximated as punctual and the sphere section reads:  $\frac{\Omega}{4\pi} = \frac{R^2}{4(R^2+d^2)}$ . The neutron sensitivity  $S$  in count per fast neutron and square centimeter is eventually derived according to (4):

$$S = \frac{\lambda \cdot \Sigma}{A \cdot \nu \cdot \frac{\Omega}{4\pi}} \quad (4)$$

thus equaling  $0.77 \pm 0.13$   $\text{c}\cdot\text{n}^{-1}\cdot\text{cm}^2$  in a cesium-137 type background ranging from 0.7 to 60  $\mu\text{Sv}\cdot\text{h}^{-1}$  and  $0.30 \pm 0.08$   $\text{c}\cdot\text{n}^{-1}\cdot\text{cm}^2$  in a cobalt-60 type background ranging from 0.6 to 35  $\mu\text{Sv}\cdot\text{h}^{-1}$ .

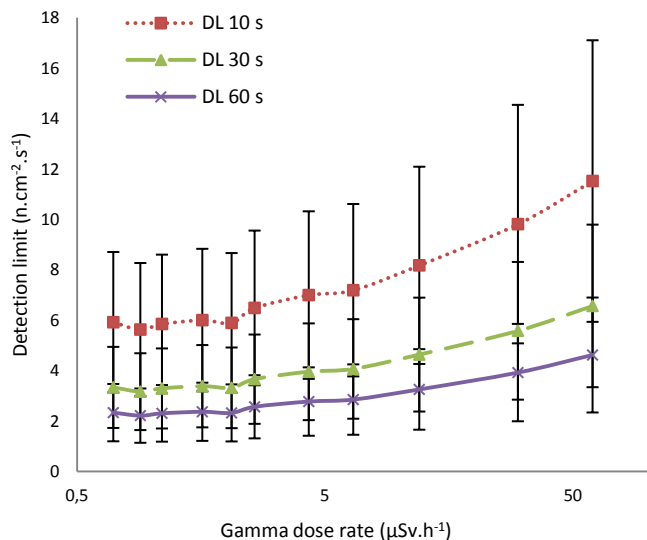
To provide a commercial reference, the same experiment was carried out with the LB 6411 Neutron Probe. The device, based on a helium-3 proportional counter inserted into a 12.5 cm radius moderator sphere, was positioned at a distance  $d = 60$  cm from the source. A neutron count rate  $\lambda = 2.4 \pm 0.1$  cps was recorded, thus allowing us to calculate a sensitivity  $S = 0.055 \pm 0.002$   $\text{c}\cdot\text{n}^{-1}\cdot\text{cm}^2$ .

### D. Detection limits

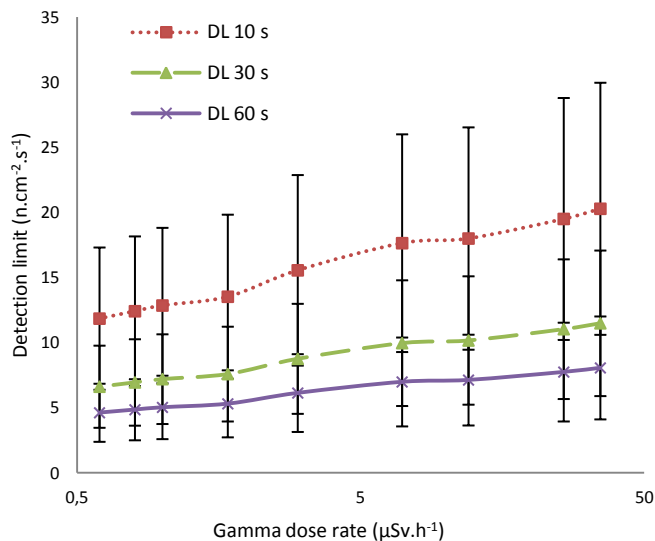
Let, for a given counting measurement, the ambient gamma dose rate be labeled  $\Delta$  and the total integration time  $t$ . For a given type of background, if the background count rate is noted  $B(\Delta)$ , the detection limit [36] in count per second  $DL$  is derived from (5):

$$DL(\Delta, t) = \frac{2.71 + 4.61\sqrt{B(\Delta)\cdot t}}{t} \quad (5)$$

264 Three realistic integration times  $t = 10$  s, 30 s, 60 s are selected, allowing for enough statistics to be gathered as well as a  
 265 responsivity meeting real-life requirements to be ensured. The evolution of the detection limit converted into neutron per  
 266 centimeter square *via* the sensitivities calculated in the previous subsection, is reported as a function of gamma dose rate in  
 267 presence of a cesium-137 and a cobalt-60 source in Fig. 12 and Fig. 13 respectively.  
 268



269 Fig. 12. Detection limits in presence of a cesium-137 background  
 270  
 271



272 Fig. 13. Detection limits in presence of a cobalt-60 background  
 273  
 274

275 These characteristics compare to the three detection limits computed from the commercial LB 6411 Neutron Probe, whose  
 276 background count rate remains stable, equal to 0.02 cps, under the same gamma source exposure: respectively  $DL = 8.7 \pm 1.9$   
 277  $\text{n}\cdot\text{cm}^{-2}\cdot\text{s}^{-1}$ ,  $DL = 3.8 \pm 1.1 \text{ n}\cdot\text{cm}^{-2}\cdot\text{s}^{-1}$  and  $DL = 2.4 \pm 0.8 \text{ n}\cdot\text{cm}^{-2}\cdot\text{s}^{-1}$  for  $t = 10$  s, 30 s and 60 s.

## 278 VII. DISCUSSION

279 The background count rate characteristic illustrated in Fig. 9 exhibits significantly non-null values, ranging from  $6.3 \pm 0.2$   
 280 cps to  $1.5 \pm 0.1$  cps for a threshold varied between 2.5 and 6 MeV, against 0.02 cps with a reference LB 6411 Neutron Probe.  
 281 This two-order of magnitude increase arises from the sensitivity to high-energy cosmic and telluric radiations, and cannot be  
 282 erased by any mere elevation of the counting threshold. However, the stability curves presented in Fig. 10 and Fig. 11 show that,  
 283 for both a cesium-137 and a cobalt-60 background, the displayed neutron counting is robust to an increase of the gamma dose  
 284 rate representing two orders of magnitude, respectively from 0.7 to 60  $\mu\text{Sv}\cdot\text{h}^{-1}$  and from 0.6 to 35  $\mu\text{Sv}\cdot\text{h}^{-1}$ . As a reminder, a  
 285 conventional environment lies under 0.5  $\mu\text{Sv}\cdot\text{h}^{-1}$  [37], while “blue” (monitored area), “green” (controlled area) and “yellow”  
 286 (specially regulated area) radioprotection zones according to legislation [38] are respectively defined from 0.5 to 7.5  $\mu\text{Sv}\cdot\text{h}^{-1}$ , 7.5  
 287 to 25  $\mu\text{Sv}\cdot\text{h}^{-1}$  and 25 to 2000  $\mu\text{Sv}\cdot\text{h}^{-1}$ . It follows that, once the inherent photon background counting has been accounted for, for

instance via a relevance threshold for the detection, the system ensures a stable counting over a broad spectrum of dose rate environments, addressing most of the security and industrial dosimetry frameworks. The neutron sensitivity of the dual sensor introduced in this paper over the addressed dose rate range varies between  $0.77 \pm 0.13 \text{ c.n}^{-1}\text{.cm}^2$  in a cesium-137 type background  $0.30 \pm 0.08 \text{ c.n}^{-1}\text{.cm}^2$  in a cobalt-60 type background, overcoming of approximately one order of magnitude the sensitivity obtained with a similar volume helium-3 Bonner sphere. This excellent sensitivity derives from the optimized implementation of the gadolinium cross section for the radiative capture of thermal neutrons and highlights the potential of gadolinium-and-plastic-based alternatives to helium-3 counters. However, because of a poorer neutron/gamma discrimination performance, this sensitivity merit is minored in the calculation of fast incident neutron flux by a higher gamma background count rate, which furthermore increases as a function dose rate (contrary to the stable helium-3 counter background count rate over the addressed range). As a consequence, the detection limits attained with our system over integration times compatible with real-life requirements compared to those achieved with a commercial helium-3 probe appear:

- in a cesium-137 environment, equivalent between  $0.5 \mu\text{Sv.h}^{-1}$  and  $7.5 \mu\text{Sv.h}^{-1}$  (blue zone), and degraded by a factor 1.5 to 2 between  $7.5 \mu\text{Sv.h}^{-1}$  and  $60 \mu\text{Sv.h}^{-1}$  (green zone and beginning of the yellow zone);
- in a cobalt-60 environment, degraded by a factor 2 to 3 between  $0.5 \mu\text{Sv.h}^{-1}$  and  $7.5 \mu\text{Sv.h}^{-1}$  (blue zone), and by a factor 3 to 3.5 between  $7.5 \mu\text{Sv.h}^{-1}$  and  $60 \mu\text{Sv.h}^{-1}$  (green zone and beginning of the yellow zone).

The gadolinium-plastic scheme therefore ensures slightly degraded detection limits within the same order of magnitude as the helium-3 Bonner sphere under the investigated gamma backgrounds for a primary cost (styrene, fluorophores, gadolinium plus mold) below 500 euro. The bias of the displayed neutron counting above  $100 \mu\text{Sv.h}^{-1}$ , which still has to be investigated, together with the resilience of the prototype to temperature and mechanical constraints, will allow the delimitation of the dose rate perimeter and therefore the exhaustive range of applications over which our instrument may constitute an effective, reliable and affordable alternative to helium-3 Bonner spheres in future years.

## VIII. CONCLUSION AND PERSPECTIVES

Both simulation and experiment results highlight the potential for a stable, highly sensitive, transportable and cost-efficient neutron detector and counter, relevant as an alternative to helium-3 and lithium-6 based Bonner spheres, for radioprotection as well as for security purposes. The degradation of the sensitivity by elevation of the counting threshold in presence of an increasing gamma dose rate results from the influence of pile-up, especially critical under high-energy backgrounds. The implementation of pile-up rejection schemes will therefore be investigated in the next developments. Further research will also be carried out around the choice of the plastic scintillator matrix and structuration of the scintillator-photomultiplier interface in order to maximize the extraction of scintillation photons.

## ACKNOWLEDGEMENTS

The authors would like to thank Frédéric Lainé, Emmanuel Rohée, Jean-Michel Bourbotte, Guillaume Sannié, Hassen Hamrita and Christian Lyron for their help in writing this paper.

## REFERENCES

- [1] J. K. Mattingly, J. March-Leuba, T. E. Valentine, J. T. Mihalezo, T. Ucklan, "Physics design of fissile mass-flow monitoring system", Instrumentation and Controls Division, Oak Ridge National Laboratory (1997).
- [2] E. Rohée, R. Coulon, C. Jammes, S. Normand, F. Carrel, F. Lainé, P. Filliatre, "Clad Failure Detection System Based on Delayed Neutron Detection without Photoneutron Noise for Sodium-Cooled Fast Reactors", *Proceeding of Nuclear Science Symposium* (2014).
- [3] D. E. Hankins, "Progress in personal neutron dosimetry", University of California, Los Alamos Scientific Laboratory (1973).
- [4] "Chemical, biological, radiological or nuclear (CBRN) detection: a technological overview", NATO Parliamentary Assembly, pp. 18-20 (2005).
- [5] "Managing critical isotopes, weaknesses in DOE's management of helium-3 delayed the federal response to a critical supply shortage", GAO-11-472, U.S. Government Accountability Office, Washington, D.C. (2011).
- [6] I. H. Campbell, B. K. Crone, "Efficient plastic scintillators utilizing phosphorescent dopants", *Applied Physics Letter* **90**, 012117 (2007).
- [7] D. A. Shea, "The helium-3 shortage: supply, demand and options for Congress", Congressional Research Service (2010).
- [8] T. Bouassoule, F. Fernández, M. Tomás, M. Bakali, P. Carmena, L. Lara, "Monte Carlo calculations and experimental calibrations of Bonner sphere systems with a new cylindrical helium-3 proportional counter", *Radiation Measurements*, **34**, pp. 199-202 (2001).
- [9] R. T. Kouzes, J. H. Ely, L. E. Erikson, W. J. Kernan, A. T. Lintereur, E. R. Siciliano, D. L. Stephens, D. C. Stromswold, R. M. Van Ginhoven, M. L. Woodring, "Neutron detection alternatives to  $^3\text{He}$ , for national security applications", *Nuclear Instruments and Methods in Physics Research Section A*, Vol. 623, pp 1035-1045 (2010).
- [10] M. Mares, H. Schraube, "Improved response matrices of Bonner spheres spectrometers with  $^6\text{LiI}$  scintillation detector and  $^3\text{He}$  proportional counter between 15 and 100 MeV", *Nuclear Instruments and Methods in Physics Research Section A*, Vol. 366, pp 203-206 (1995).
- [11] D. A. Abdushukurov, *Gadolinium foils as converters of thermal neutrons in detectors of nuclear radiation*, Physics Research and Technology, p. 7 (2010).
- [12] A. M. Williams, P. A. Beeley, N. M. Spyrou, "Response of Lithium Gadolinium Borate in monoenergetic neutron fields", *Radiation Protection Dosimetry*, Vol. 110, Nos 1-4, pp. 497-502 (2004).
- [13] B. La Course, A. Hardy, H. Rétot, Q. Chen, X. Peng, B. Vlana, M. Zandi, "Ceramic scintillator body and scintillator device", US 2012/0049118 A1 Patent (2012).

- 346 [14] C. Greskovitch, S. Duclos, "Ceramic scintillators", *Annu. Rev. Mater. Sci.* **27**, 69-88 (2007).
- 347 [15] R. G. Downing, W. B. Feller, "Radiation detectors and methods of detecting radiation", US 7233007 B2 Patent (2007).
- 348 [16] H. Beil, R. Bergère, A. Veyssière, "Détection de photoneutrons avec un scintillateur liquide chargé au gadolinium", *Service de Physique*
- 349 *Appliquée*, Tome 4, pp. 249-250 (1969).
- 350 [17] S. Normand, V. Kondrasovs, G. Corre, J.-M. Bourbotte and A. Ferragut, "MA-NRBC: First successful attempt for neutron gamma
- 351 discrimination in plastic scintillators", *Proceeding of Advancements in Nuclear Instrumentation Measurement Methods and their*
- 352 *Applications* (2011).
- 353 [18] M. A. Osinski, B. A. Akins, J. B. Plumley, A. C. Rivera, G. A. Smolyakov, J. M. Vargas, N. J. Withers, "Thermal neutron detectors based
- 354 on gadolinium-containing nanoscintillators", US 2012/0286166 A1 Patent (2012).
- 355 [19] M. Hamel, G.H.V. Bertrand, F. Carrel, R. Coulon, J. Dumazert, E. Montbarbon and F. Sguerra, "Current status on plastic scintillators
- 356 modifications", *Proceeding of Advancements in Nuclear Instrumentation Measurement Methods and their Applications* (2015).
- 357 [20] N. J. Hogan, *Characterization of a Cadmium Capture-gated Neutron Spectrometer*, Department of Physics and Astronomy, Brigham
- 358 Young University, pp. 22-25 (2011).
- 359 [21] W. J. Richard, "Scintillator detector with gadolinium-based sidewall axial restraint and compliance assembly", EP 1403661 A1 Patent
- 360 (2004).
- 361 [22] R. de Vita, F. Ambi, M. Battaglieri, M. Osipenko, D. Piombo, G. Ricco, M. Ripani, M. Taiuti, "A large surface neutron and photon
- 362 detector for civil security applications", *Nuclear Instruments and Methods in Physics Research A*, **617**, 219-222 (2010).
- 363 [23] R. M. Polichar, J. Baltgalvis, "Neutron detector with layered thermal neutron scintillator and dual function light guide and thermalizing
- 364 media", US 2005/0224719 A1 Patent (2005).
- 365 [24] A. Alemberti, M. Battaglieri, E. Botta, R. de Vita, E. Francini, G. Firpo, "SCINTILLA : A European project for the development of
- 366 scintillation detectors and new technologies for nuclear security", *WSPC – Proceedings* (2014).
- 367 [25] J. Dumazert, F. Carrel, R. Coulon, M. Hamel, Commissariat à l'Energie Atomique et aux Energies Alternatives, "Dispositif de détection
- 368 de neutrons thermiques comportant une coquille de scintillateur plastique enveloppant un cœur de gadolinium ou de cadmium et dispositif
- 369 de comptage de neutrons thermiques associé", FR 1552110 Patent application (2015).
- 370 [26] Radioprotection: Radio-nucléides, Thorium-232, Institut de Radioprotection et de Sûreté Nucléaire, ED 4317 (2013).
- 371 [27] [www.nds.iaea.org.htm](http://www.nds.iaea.org.htm)
- 372 [28] *MCNPX User Manual*, Los Alamos Tech. rep., LA-CP-11-00438, Los Alamos (2011).
- 373 [29] M. Benmosbah, *Spectrométrie des neutrons : étude de la réponse d'un ensemble de compteurs proportionnels*, Université de Franche-
- 374 Comté (2007).
- 375 [30] G. H. V. Bertrand, J. Dumazert, F. Sguerra, R. Coulon, G. Corre and M. Hamel, "Understanding behavior of different metals in loaded
- 376 scintillators: discrepancy between gadolinium and bismuth", *Journal of Materials Chemistry C*, Vol. 3, pp. 6006-6011 (2015).
- 377 [31] [www.strem.com/catalog/v/93-6432/22/gadolinium\\_7440-54-2](http://www.strem.com/catalog/v/93-6432/22/gadolinium_7440-54-2).
- 378 [32] S. Normand, V. Kondrasovs, G. Corre, K. Boudergui, N. Blanc de Lanaute, J.-M. Bourbotte, R. Woo, P. Pin, L. Tondut, "PING for
- 379 Nuclear Measurements: First Results", *IEEE Transactions on Nuclear Science*, 59 (4) (2011).
- 380 [33] M. Bertolaccini, S. Cova, C. Bussolati, "A technique for absolute measurement of the effective photoelectron per keV yield in scintillation
- 381 counters", *Proc. Nucl. Symp.*, Versailles, France (1968).
- 382 [34] J. B. Birks, *The theory and Practice of Scintillation Counting*, Pergamon Press, pp. 97-98, pp. 185-188 (1964).
- 383 [35] R. C. Martin, J. B. Knauer, P. A. Balo, "Production, Distribution, and Applications of Californium-252 Neutron Sources", *Applied*
- 384 *Radiation and Isotopes*, vol. 53, pp. 785-792 (1999).
- 385 [36] G. R. Gilmore, *Practical Gamma-ray spectrometry*, 2<sup>nd</sup> Edition, John Wiley & Sons Ltd, The Atrium, Southern Gate, Chichester, West
- 386 Sussex, England, p.117 (2008).
- 387 [37] "American national standard for evaluation and performance of radiation detection portal monitors for use in homeland security," ANSI
- 388 N42.35 (2006).
- 389 [38] Légifrance, Arrêté du 15 mai 2006 relatif aux conditions de délimitation et de signalisation des zones surveillées et contrôlées et des zones
- 390 spécialement réglementées ou interdites compte tenu de l'exposition aux rayonnements ionisants, ainsi qu'aux règles d'hygiène, de sécurité
- 391 et d'entretien qui y sont imposées (2006), derived from : The 2007 Recommendations of the International Commission on Radiological
- 392 Protection, ICRP Publication 103, *Ann. ICRP* **37** 2-4 (2007).
- 393
- 394
- 395
- 396
- 397